6470–6479 *Nucleic Acids Research, 2018, Vol. 46, No. 13* *Published online 13 June 2018*
doi: 10.1093/nar/gky499

Hg^{II} binds to C–T mismatches with high affinity

Olivia P. Schmidt, Andrea S. Benz, Guillaume Mata and Nathan W. Luedtke*

University of Zurich, Department of Chemistry, Zurich, Switzerland

Received March 14, 2018; Revised May 04, 2018; Editorial Decision May 20, 2018; Accepted June 11, 2018

ABSTRACT

Binding reactions of Hg^{II} and Ag^{I} to pyrimidine-pyrimidine mismatches in duplex DNA were characterized using fluorescent nucleobase analogs, thermal denaturation and ^{1}H NMR. Unlike Ag^{I}, Hg^{II} exhibited stoichiometric, site-specific binding of C–T mismatches. The on- and off-rates of Hg^{II} binding were approximately 10-fold faster to C–T mismatches ($k_{on} \approx 10^{5}$ M^{-1} s^{-1}, $k_{off} \approx 10^{-3}$ s^{-1}) as compared to T–T mismatches ($k_{on} \approx 10^{4}$ M^{-1} s^{-1}, $k_{off} \approx 10^{-4}$ s^{-1}), resulting in very similar equilibrium binding affinities for both types of 'all natural' metallo base pairs (K_d ≈ 10–150 nM). These results are in contrast to thermal denaturation analyses, where duplexes containing T–T mismatches exhibited much larger increases in thermal stability upon addition of Hg^{II} (ΔT_m = 6–19°C), as compared to those containing C–T mismatches (ΔT_m = 1–4°C). In addition to revealing the high thermodynamic and kinetic stabilities of C–Hg^{II}–T base pairs, our results demonstrate that fluorescent nucleobase analogs enable highly sensitive detection and characterization of metal-mediated base pairs – even in situations where metal binding has little or no impact on the thermal stability of the duplex.

INTRODUCTION

First reported in the early 1960s (1–3), T–Hg^{II}–T base pairs provided the first examples of 'all natural' metal-mediated base pairs composed of pyrimidine-pyrimidine mismatches coordinated to a transition metal ion. High-resolution structural studies revealed that mercury(II) ions bind to T–T mismatches via *N3* coordination of two deprotonated thymidine residues (Figure 1A) (4). Structurally analogous C–Ag^{I}–C base pairs have also been well characterized (5). In both cases, little or no impact on the global structure of the B-form duplex was observed (4–7). A wide variety of other metallated base pairs have been observed in crystals of non-B-form nucleic acids (8–10). For example, a G–Au^{III}–C base pair was observed in the initiation site of HIV-1 RNA (11), and a C–Hg^{II}–T base pair was found in short, A-form duplex DNA where the metal ion was unexpectedly bound to the exocyclic amine (*N4*) of a deprotonated cytosine residue and to the *N3* of a deprotonated thymidine (9). A solid-state 'wire' containing C–Ag^{I}–C, G–Ag^{I}–G, G–Ag^{I}–C, and T–Ag^{I}–T base pairs was recently reported (8), as well as a short, non-helical DNA structure containing one G–Ag^{I}–G and two C–Ag^{I}–C base pairs (10). In most such cases, very little or nothing is known about the kinetic or thermodynamic parameters of metallo base pair formation in solution.

All natural, metal-mediated base pairs are potentially important in both biological and materials sciences (12–25). A detailed understanding of their kinetic and thermodynamic properties is essential for gauging their potential applications in devices as well as their ability to interfere with biological processes (26–29). The energetics of metallo base pair formation has been characterized using a wide variety of techniques (30–44). High affinity, stoichiometric binding of Hg^{II} and Ag^{I} to DNA duplexes containing T–T or C–C mismatches was initially revealed using thermal denaturation studies, isothermal titration calorimetry and ^{1}H NMR spectroscopy (36–42). Remarkably, duplexes containing T–Hg^{II}–T base pairs or C–Ag^{I}–C base pairs exhibited similar thermal stabilities as duplexes containing canonical T–A or G–C base pairs (38,39). In contrast, little or no change was observed in the thermal melting temperatures of duplexes containing C–T mismatches upon addition of Hg^{II} (44). This result could be interpreted as the absence of a strong binding interaction, however, in some cases, high-affinity metal binding can decrease the thermal stability of duplex DNA (45,46).

Fluorescent nucleobase analogs provide highly sensitive probes for the real-time study of molecular binding interactions (47–57). In contrast to NMR, isothermal calorimetry, and absorbance-based thermal denaturation analyses, very dilute (nM) solutions of fluorescent nucleic acids can be used to directly characterize the thermodynamic and kinetic parameters of DNA-metal binding reactions (29,58–60). In practice, this enables the measurement of equilibrium binding constants (K_d) in the low nM range, something that is not feasible by analyzing binding data collected using DNA solutions in the μM to mM concentration range. This limitation is especially relevant to the characterization of metal-DNA binding interactions, where non-specific Hg^{II}

*To whom correspondence should be addressed. Tel: +41 44 635 4244; Fax: +41 44 635 6891; Email: nathan.luedtke@chem.uzh.ch
Present address: Nathan W. Luedtke. Department of Chemistry, University of Zurich, Winterthurerstrasse 190, CH-8057 Zurich, Switzerland.

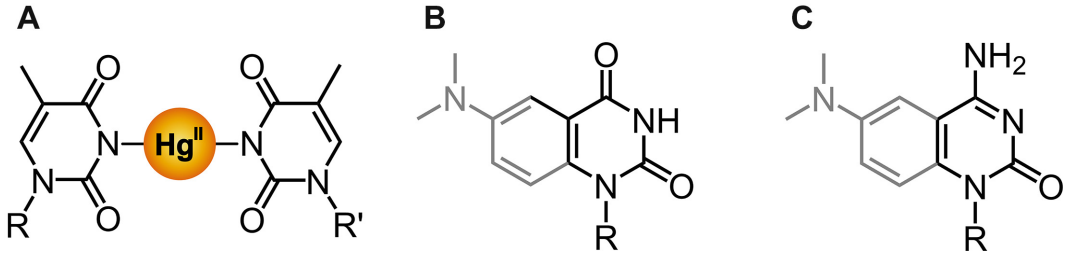

Figure 1. (**A**) T–Hg^{II}–T base pair (4). (**B**) Fluorescent thymidine analog ^{DMA}**T** (43). (**C**) Fluorescent cytosine analog ^{DMA}**C** (61).

binding by canonical, duplex DNA occurs with relatively high affinity (K_d = 0.2–2.0 μM in non-coordinating and metal-coordinating buffers, respectively) (29). We recently reported a novel fluorescence-based assay to investigate site-selective T–Hg^{II}–T base pair formation using the fluorescent nucleobase analog ^{DMA}**T** (Figure 1B) (43). By monitoring the real-time changes in ^{DMA}**T**-fluorescence upon addition of Hg^{II} or a Hg^{II} scavenger, the Hg^{II} binding affinities (K_d), and association/dissociation rate constants (k_{on} and k_{off}) of T–T mismatches were determined under various conditions (29). Even in the presence of metal-coordinating buffers containing phosphate and citrate, T–Hg^{II}–T base pairs exhibited high thermodynamic stabilities (K_d = 8–50 nM) and high kinetic stabilities (half-lives = 0.3–1.3 h) that interfered with dynamic processes such as DNA–DNA strand displacement and enzymatic primer extension reactions. The use of non-coordinating buffers such as sodium cacodylate had little impact on the thermodynamic or kinetic stabilities of T–Hg^{II}–T base pairs, but caused a 10-fold increase in the non-specific binding affinity of Hg^{II} to duplexes lacking a base pair mismatch (29).

Here, we report the use of DNA duplexes containing a fluorescent thymidine mimic ^{DMA}**T** (43), or an analogous cytosine mimic ^{DMA}**C** (61) (Figure 1C) to evaluate site-selective metal binding of Hg^{II} or Ag^{I} to C–T mismatches. Together with ^{1}H NMR experiments, our results demonstrate that Hg^{II}, but not Ag^{I}, exhibits high-affinity, stoichiometric binding of C–T mismatches in duplex DNA, with thermodynamic stabilities (K_d = 10–153 nM) very similar to those of widely-studied T–Hg^{II}–T base pairs (29). These affinities are ∼10–200 times higher than non-specific binding of Hg^{II} to duplexes lacking a mismatch ($K_d \approx 2$ μM) in a metal-coordinating buffer containing citrate and phosphate. Remarkably, temperature-dependent K_d measurements revealed that C–T mismatches exhibited a three-fold *higher* Hg^{II} affinity at 4°C versus 25°C, whereas T–T mismatches exhibited a 2-fold *lower* Hg^{II} affinity at 4°C versus 25°C. Taken together, these results suggest that the less favorable entropy changes of C–Hg^{II}–T versus T–Hg^{II}–T formation are responsible for the negligible impact that Hg^{II} had on the thermal stabilities of DNA duplexes containing C–T mismatches (ΔT_m = 1–4°C) as compared to T–T mismatches (ΔT_m = 6–19°C). In addition to revealing the high thermodynamic and kinetic stabilities of C–Hg^{II}–T base pairs, our results have revealed that the on- and off-rates of Hg^{II} binding were approximately 10-fold faster to C–T mismatches ($k_{on} \approx 10^5$ M^{-1} s^{-1}, $k_{off} \approx 10^{-3}$ s^{-1}) as compared to T–T mismatches ($k_{on} \approx 10^4$ M^{-1} s^{-1}, $k_{off} = 10^{-4}$ s^{-1}). Taken together with the differences in their formation entropies, these results suggest that C–Hg^{II}–T and T–Hg^{II}–T base pairs exhibit different metal binding modes.

MATERIALS AND METHODS

Oligonucleotide synthesis, names and sequences

DNA oligonucleotides (21-mers) containing a single ^{DMA}**T** at a variable position '**X**' were synthesized using phosphoramidite chemistry, purified and characterized as previously reported (43). ^{DMA}**C**-containing oligonucleotides were synthesized using the previously reported ^{DMA}**C** phosphoramidite (61). To avoid ^{DMA}**C** deamination, automated DNA synthesis was performed under 'ultramild' conditions (62), and the oligonucleotides were deprotected and cleaved from the resin using K_2CO_3 in MeOH at r.t. for 5.5 h. Unmodified oligonucleotides were purchased from *Sigma-Aldrich* as HPLC-purified products. DNA names and sequences of 21-mers containing a single site of modification by ^{DMA}**T** or ^{DMA}**C**: **X13**: 5′-CCC–TAA-CCC–TAA-**X**CC–TAA-CCC-3′; **X14**: 5′-CCC–TAA-CCC–TAA-C**X**C–TAA-CCC-3′; **X15**: 5′-CCC–TAA-CCC–TAA-CC**X**-TAA-CCC-3′. DNA names and sequences of unmodified, self-complementary 14-mers containing two mismatches (bold): ODN[15] **'C–T'**: 5′-CG-T**C**T CAT-GA**T**-ACG-3′; ODN[16] **'T–T'**: 5′-CG-T**T**T-CAT-GA**T**-ACG-3′. See Supplementary Tables S1 and S2 (Supplementary Information) for a complete list of duplexes. Oligonucleotide stock solutions were prepared in deionized water and their concentrations determined by absorbance at 260 nm using molar extinction coefficients (ε_{260}) calculated using a nearest-neighbor model (63,64). The extinction coefficients of ^{DMA}**T**- and ^{DMA}**C**-containing oligonucleotides were calculated using the base composition method by multiplying the sum of the coefficients of the individual nucleosides by a factor of 0.9 to account for base stacking interactions (65). Double-stranded oligonucleotides were prepared from equal amounts of complementary oligonucleotides in the indicated aqueous buffer by heating to 95°C for 5 min, followed by slow cooling to room temperature over 4 h. For self-complementary sequences, oligonucleotides were diluted in the indicated buffer and annealed as above.

Metal ion screening by fluorescence

Pre-folded duplex '**X14**' (8 μM) in aqueous buffer (200 mM of Na_2HPO_4, 100 mM of citric acid and 100 mM $NaNO_3$ (pH 7.35)) was mixed 1:1 (v:v) with solutions of metal ions

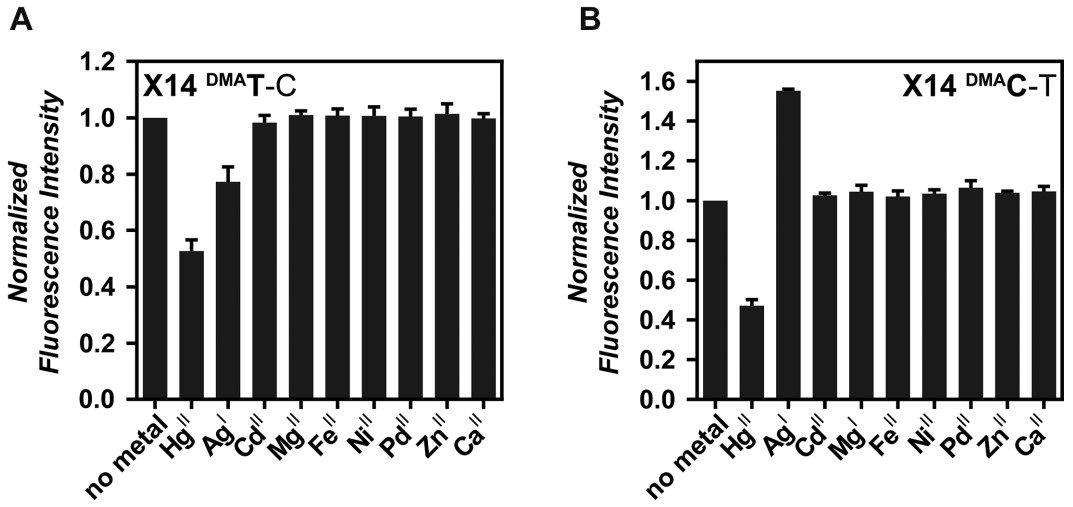

Figure 2. (**A**) Fluorescence changes of duplex **X14** containing a ^{DMA}**T**–C mismatch, or, (**B**) ^{DMA}**C**–T mismatch upon addition of various metal ions (2.0 equiv). The addition of Hg^{II} to duplexes **X13** or **X15** containing a ^{DMA}**T**–G mismatch or a ^{DMA}**T**–A base pair resulted in minimal changes in fluorescence intensity (Supplementary Figure S1, SI). All samples contained 4 μM of DNA in aqueous buffer (200 mM of Na_2HPO_4, 100 mM of citric acid and 100 mM $NaNO_3$ (pH 7.35)) and were incubated with metal ions for 3 h prior to measuring. For duplex sequences see Supplementary Table S1, SI.

in the same buffer to a final concentration of 4 μM DNA and 8 μM of $Hg(ClO_4)_2$, $AgNO_3$, $CdCl_2$, $MgCl_2$, $FeCl_2$, $NiCl_2$, $Pd(NO_3)_2$, $ZnCl_2$ or $CaCl_2$ and incubated at r.t. for 3 h prior to each measurement. Fluorescence spectra were recorded at 25°C using a *Molecular Devices Spectra spectrofluorophotometer* with a temperature controller in 96- or 384-well plates.

NMR studies

Duplex DNA (0.5 mM) was prepared by dissolving 1.0 mM of the self-complementary sequence ODN[15] '**C–T**' in aqueous buffer (200 mM $NaClO_4$, 50 mM cacodylic acid in H_2O/D_2O (9:1) at pH 7.0, heating to 95°C for 5 min, and slowly cooling to r.t. over 4 h. Samples were equilibrated at 4°C for 20 min prior to measuring. For Hg^{II} titration experiments, aliquots of $Hg(ClO_4)_2$ were added, and the NMR-spectra were recorded after incubating each sample for 15 min at r.t. followed by 15 min at 4°C. ^{1}H NMR spectra were recorded on a Bruker Avance II 500 MHz spectrometer equipped with a TXI *z*-axis gradient probe head using excitation sculpting for water suppression. Proton chemical shifts were referenced to the water line at 4.70 ppm. The spectra were processed with a line broadening factor of 10 Hz.

Thermal melting analyses (T_m)

Melting temperatures (T_m) of self-complementary sequences were determined from the changes in absorbance at 260 nm as a function of temperature in a 1 mm path length thermo-controlled, strain-free quartz cuvette on a *JASCO J-715* spectrometer equipped with a temperature control system. Solutions of pre-folded duplex DNA in aqueous buffer (200 mM $NaClO_4$, 50 mM cacodylic acid at pH 7.0) were equilibrated at 4°C for 20 min and slowly ramped to 90°C with 0.5°C steps at a rate of 25°C/h. Where indicated, DNA samples were incubated with 2.0 equiv (relative to mismatch) of $Hg(ClO_4)_2$ or $AgNO_3$ for 3 h prior to analysis. T_m values were calculated as the first derivatives of both the heating and cooling curves measured in triplicate and averaged. Little or no hysteresis ($\leq$1.0°C) was observed between each heating and cooling cycle. Melting temperatures (T_m) of 21-mer duplexes **X13**, **X14** and **X15** were determined from changes in the molar ellipticity at 262 nm as a function of temperature in a 1 mm path length thermo-controlled, strain-free quartz cuvette on a *JASCO J-715* spectrometer. A 5 μM solution of pre-folded duplex DNA in aqueous buffer (200 mM of Na_2HPO_4, 100 mM of citric acid and 100 mM $NaNO_3$ (pH 7.35)) was equilibrated for 15 min at 5°C and slowly ramped to 95°C at a rate of 10°C/h. T_m values were determined by plotting the molar ellipticity versus temperature using a dose–response non-linear regression and were calculated from the averaged values of heating and cooling curves. Where indicated, duplex DNA was annealed in the presence of 1.0 equiv of $Hg(ClO_4)_2$. The reproducibility of the measurement was within 0.3°C.

Circular dichroism (CD) spectroscopy

Circular dichroism spectra of pre-annealed duplex DNA were measured at 25°C using a 2 nm band width with 0.1 nm steps at a scanning rate of 20 nm / min in a 1 mm path length thermo-controlled strain-free quartz cuvette on a *JASCO J-715* spectrometer. Self-complementary duplex DNA (10 μM) was prepared by diluting the self-complementary sequences into aqueous buffer (200 mM $NaClO_4$, 50 mM cacodylic acid at pH 7.0), heating to 95°C for 5 min, and slowly cooling to room temperature over 4 h. The final pH was then adjusted to 7.8 by adding a solution of NaOH. Duplex DNAs analyzed in the presence of Hg^{II} were incubated with $Hg(ClO_4)_2$ for 3 h prior to use. 21-mer duplexes **X13**, **X14** and **X15** (5 μM) were annealed in the presence or absence of 1.0 equiv of $Hg(ClO_4)_2$ in aqueous buffer (200 mM of Na_2HPO_4, 100 mM of citric acid and 100 mM $NaNO_3$

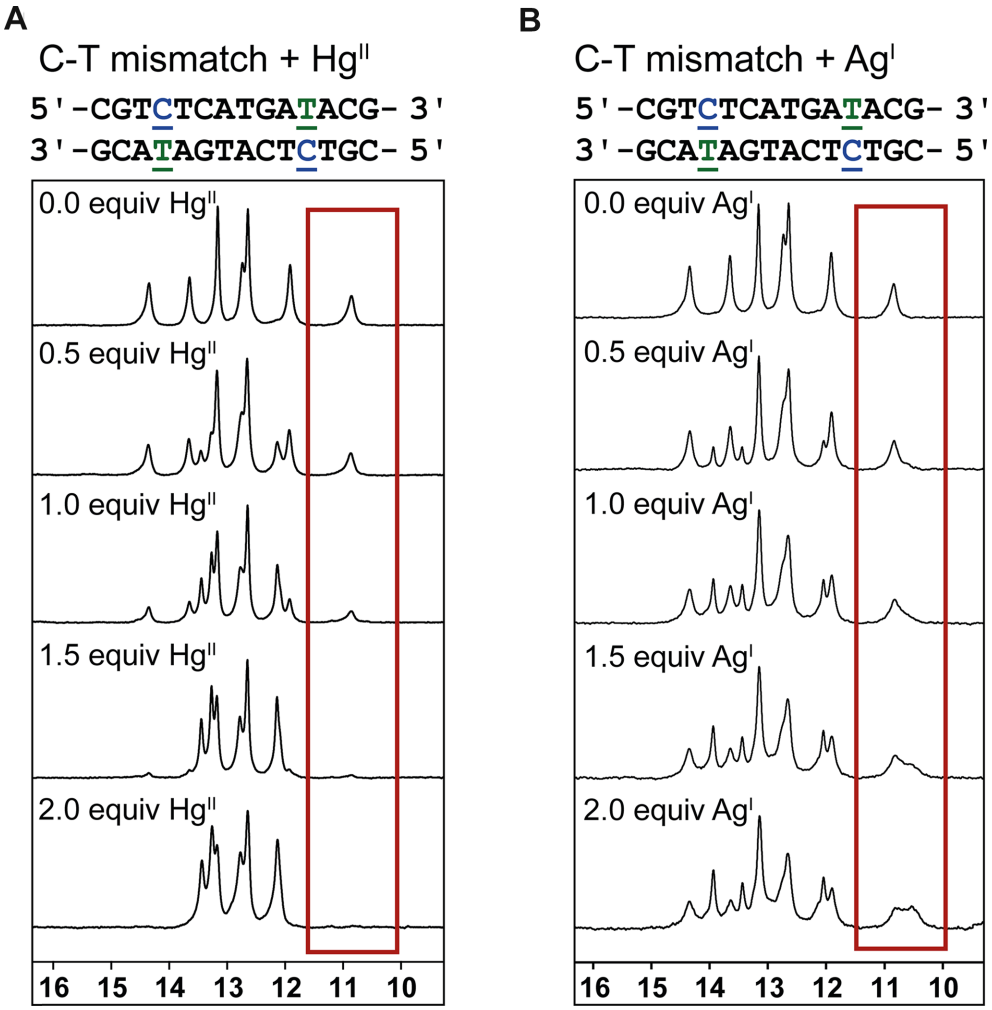

Figure 3. (**A**) Site-specific binding of Hg^{II} to C–T mismatches in 14-mer duplex DNA (ODN^{15} '**C–T**') according to disappearance of imino-resonance of the mismatched thymidine upon addition of Hg^{II}. (**B**) Heterogenous binding of Ag^{I} to the same DNA upon addition of Ag^{I}. The number of metal ion equivalents are with respect to the number of mismatches present in the DNA. Samples were measured at 4°C and contained 0.5 mM of pre-folded duplex DNA in aqueous buffer (200 mM $NaClO_4$, 50 mM cacodylic acid at pH 7.0).

(pH 7.35)). CD spectra were recorded as described above, except that a scanning rate of 50 nm/min was used.

Rate constant (k_{on} and k_{off}) measurements

Rate constants of Hg^{II} association (k_{on}) were determined as previously reported (29) in three independent trials using a *Horiba* FluoroLog spectrofluorophotometer equipped with a speed stirrer and a temperature controller. Pre-annealed duplex DNA (4 μM) in aqueous buffer (200 mM of Na_2HPO_4, 100 mM of citric acid and 100 mM $NaNO_3$ (pH 7.35)) was diluted to 0.1 μM in the same buffer in a 1.5 ml cuvette. Changes in fluorescent intensity were measured as a function of time (λ_{ex} = 370 nm, λ_{em} = 500–510 nm) upon adding 2, 4 or 6 equiv of Hg^{II} while stirring at 25°C. Rate constants of Hg^{II} dissociation (k_{off}) were determined as previously reported (29) in three independent trials using a 1.5 ml cuvette as above, or using 384-well plates and a *Molecular Devices SpectraMax M5 spectrofluorophotometer* equipped with a temperature controller. Pre-annealed duplex DNA samples (prepared at 4 or 8 μM) were incubated with 2 equiv of Hg^{II} for 3h. Changes in fluorescent intensity then were measured as a function of time (λ_{ex} = 370 nm, λ_{em} = 500–510 nm) upon adding 50 equiv of 'scavenger DNA' at 25°C. The final concentration of fluorescent DNA was 0.1 or 4 μM in aqueous buffer ((200 mM of Na_2HPO_4, 100 mM of citric acid and 100 mM $NaNO_3$ (pH 7.35)). Samples measured in 384-well plates were overlaid with paraffin oil. The observed dissociation rates were independent of the fluorescent DNA concentrations in this range.

Equilibrium binding affinity (K_d) measurements

Equilibrium binding affinities (K_d) were determined as previously reported (29) in three independent trials using a *Horiba* FluoroLog spectrofluorophotometer. Pre-annealed duplex DNA (4 μM) was diluted to 25 nM in aqueous buffer (200 mM of Na_2HPO_4, 100 mM of citric acid and 100 mM $NaNO_3$ (pH 7.35) in a 1.5 ml cuvette. Aliquots of $Hg(ClO_4)_2$ were added while stirring at 4 or 25°C and

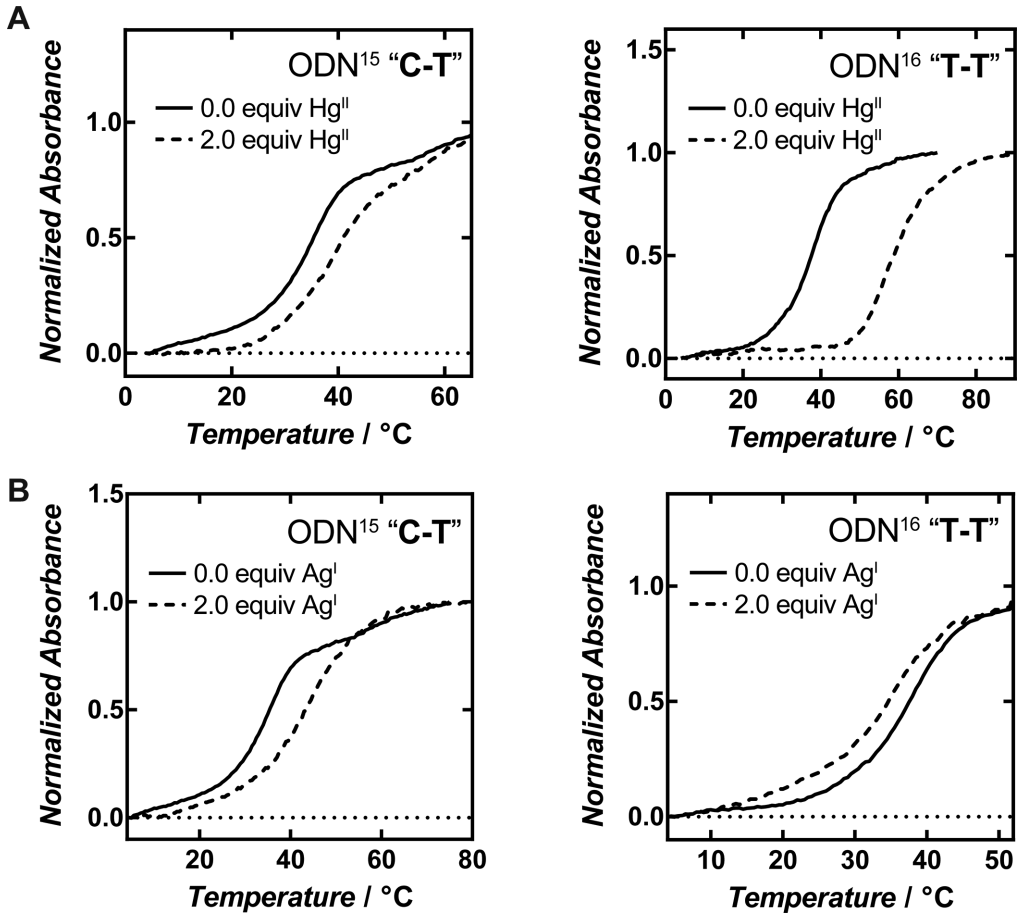

Figure 4. Thermal denaturation curves of (**A**) ODN^{15} '**C–T**' (left) and ODN^{16} '**T–T**' (right) in the presence and absence of 2.0 equiv of Hg^{II}, and, (**B**) ODN^{15} '**C–T**' (left) and ODN^{16} '**T–T**' (right) in the presence and absence of 2.0 equiv of Ag^{I}. The equivalents of each metal ion are with respect to the number of mismatches present. DNA samples contained 10 μM of pre-folded, 14-mer duplex DNA in aqueous buffer (200 mM $NaClO_4$, 50 mM cacodylic acid at pH 7.0).

the fluorescence intensities of each concentration were measured after 30 min of equilibration.

RESULTS

Metal ion screening

Fluorescent nucleobase analogs provide highly sensitive and rapid means to screen for new metal-nucleobase binding reactions (57–60). To evaluate the abilities of metals to selectively bind to C–T mismatches in duplex DNA, 2.0 equiv of various metal ions (Hg^{II}, Ag^{I}, Cd^{II}, Mg^{II}, Fe^{II}, Ni^{II}, Pd^{II}, Zn^{II} or Ca^{II}) were incubated with pre-formed duplexes '**X14**' containing either a ^{DMA}**T**–C or ^{DMA}**C**–T mismatch. Among the metal ions evaluated, only Hg^{II} and Ag^{I} caused significant changes in fluorescence intensities (Figure 2). Consistent with the formation of ^{DMA}**T**–Hg^{II}-C and ^{DMA}**C**–Hg^{II}–T base pairs, the addition of Hg^{II} caused fluorescence quenching of both duplexes. In contrast, Ag^{I} ions caused fluorescence quenching of the duplex containing ^{DMA}**T**–C, yet enhanced fluorescence of the ^{DMA}**C**–T duplex. This unexpected enhancement is not consistent with direct ^{DMA}**C**–Ag^{I} binding, as the titration of Ag^{I} to solutions of free ^{DMA}**C** nucleoside caused fluorescence quenching (Supplementary Figure S2, SI).

^{1}H NMR titrations

To further evaluate C–Hg^{II}–T and C–Ag^{I}–T formation, we monitored imino-proton resonances (38,66) of a 14-mer, palindromic DNA (67) containing two C–T-mismatches (ODN^{15} '**C–T**') upon addition of Hg^{II} or Ag^{I} at 4°C (Figure 3). Temperature and DNA concentration-dependent CD measurements confirmed this sequence forms a stable, intermolecular duplex at temperatures $\leq$ 20°C (Supplementary Figure S3 and Supplementary Table S3, SI). In the absence of Hg^{II}, an imino-proton signal was observed at 10.9 ppm, corresponding to the mismatched thymidine *NH* (38,66,67). The addition of two equivalents of Hg^{II} (1:1 with respect to the number of mismatches present) caused stoichiometric disappearance of this unpaired thymidine *NH*-resonance. Some shifting of the other signals was also observed, but the total number of imino protons remained six upon saturation with Hg^{II} (Figure 3A). Taken together, these results indicate site-specific binding of Hg^{II} to the mismatched T. In contrast, the addition of $AgNO_3$ did not result in the disappearance of the unpaired thymidine *NH*-resonance, instead giving a complex mixture of new imino signals (Figure 3B). Taken together with the results of our fluorescence-based screening, these NMR data are consistent with the forma-

Table 1. Melting temperatures (T_m) of duplex DNA containing C–T, G-T or T–T mismatches or A–T base pairs in the presence and absence of 2 equiv of Hg^{II} and Ag^{I}[a]

Sequence	T_m (°C) no metal ions	T_m (°C), (ΔT_m) with Hg^{II}	T_m (°C), (ΔT_m) with Ag^{I}
ODN[15] '**C–T**'	35.1 ± 0.3	39.3 ± 0.2 (+4.2)	44.0 ± 0.2 (+8.9)
ODN[16] '**T–T**'	37.9 ± 0.1	57.3 ± 0.1 (+19.4)	36.2 ± 0.5 (−1.7)
ODN[17] '**G–T**'	47.3 ± 0.4	41.6 ± 0.8 (−5.7)	45.5 ± 0.4 (−1.8)
ODN[18] '**A–T**'	57.1 ± 0.1	53.2 ± 0.8 (−3.9)	57.2 ± 0.7 (+0.1)

[a] Reported values = mean ± standard deviation from three independent measurements. ΔT_m reflects the difference in T_m upon addition of 2 equiv metal ions per mismatch present. All samples contained 10 μM of duplex DNA in aqueous buffer (200 mM $NaClO_4$, 50 mM cacodylic acid at pH 7.0). For duplex sequences see Figure 3A and Supplementary Table S2, SI. For raw melting data see Figure 4 and Supplementary Figures S4 and S5, SI.

tion of site-specific, 1:1 complexes between Hg^{II} and C–T mismatches, but not between Ag^{I} and C–T mismatches.

Thermal denaturation studies

Thermal denaturation studies are widely used to investigate formation of metal-mediated base pairs in duplex DNA (36). Thermal melting temperatures (T_m) were determined using palindromic 14-mer duplex DNAs containing two C–T, T–T or G-T mismatches or two canonical A–T base pairs upon addition of Hg^{II} or Ag^{I} (Supplementary Figures S4 and S5, SI). As expected from previous studies (38), the addition of Hg^{II} to ODN[16] duplex '**T–T**' induced a large increase in melting temperature (ΔT_m = +19.4°C), yet only a small increase in T_m was observed for ODN[15] duplex '**C–T**' (ΔT_m = +4.2°C, Figure 4, Table 1). Hg^{II} caused small *decreases* in T_m values of a similar magnitude (ΔT_m = –3.9 and –5.7°C) for ODN[18] '**A-T**' and ODN[17] '**G-T**', respectively. Melting experiments conducted using 21-mer duplexes **X13**, **X14** and **X15** revealed little or no changes in melting temperatures upon addition of Hg^{II} to duplexes containing a single C–T mismatch (ΔT_m = –0.1 to +0.7°C), and much larger changes (ΔT_m = +2.9 to +6.0°C) upon addition of Hg^{II} to the duplexes containing a single T–T mismatch (Supplementary Figure S6 and Supplementary Table S4, SI). According to CD spectroscopy, the addition of Hg^{II} caused little or no change in the global structures of B-form duplexes ODN[15], **X13**, **X14** and **X15** containing C–T mismatches (Supplementary Figures S7 and S8, SI). Taken together with previous studies (36,43), these results demonstrate that the formation of C–Hg^{II}–T base pairs have little or no impact on the thermal stability of B-form duplex DNA containing C–T mismatches. This lack of thermal stabilization is in stark contrast to the high affinity, stoichiometric binding of Hg^{II} to C–T according to our fluorescence screening and ^{1}H NMR experiments. To the best of our knowledge, there are no previous reports of the thermodynamic or kinetic parameters of Hg^{II} binding to C–T mismatches in DNA or RNA.

Association and dissociation rate constants of Hg^{II} binding C–T mismatches

To evaluate the kinetic parameters of C–Hg^{II}–T formation, the changes in fluorescence intensities of 21-mer duplex DNA **X13** or **X15** containing a single ^{DMA}**T**–C mismatch, ^{DMA}**C**–T mismatch, or a wild-type C–T mismatch placed adjacent to a ^{DMA}**C**–G base pair were monitored as a function of time and Hg^{II} concentration (Figure 5a, Supplementary Figures S9–S12, SI). Rate constants of association (k_{on}) were determined using pseudo-first-order approximations (eq 1–4, SI). For all four constructs evaluated, the second-order rate constants of Hg^{II} association to C–T mismatches were in a similar range of 7.6×10^4–8.5×10^5 M^{-1} s^{-1} (Table 2). ^{DMA}**C**-containing duplexes lacking a C–T mismatch exhibited little or no time-dependent quenching under the same conditions (Supplementary Figure S12, SI).

To evaluate the rates of Hg^{II} dissociation from C–T mismatches, pre-formed duplexes containing a single ^{DMA}**T**–Hg^{II}-C, ^{DMA}**C**–Hg^{II}–T or wild-type C–Hg^{II}–T complex adjacent to a ^{DMA}**C**–G base pair were monitored upon addition of 50 equiv of a non-fluorescent, passive Hg^{II} 'scavenger' DNA containing two C–T mismatches (ODN[14], Supplementary Table S1, SI). Consistent with the dissociation of Hg^{II}, increased fluorescence was observed as a function of time (Figure 5B, Supplementary Figures S13 and S14, SI). Control experiments revealed that the use of 30, 40 and 50 equiv of scavenger gave the same apparent first-order rates (Supplementary Figure S13, SI). Data obtained using 50 equiv of scavenger DNA were fit to monoexponential curves (eq 5–7, SI) and the first-order dissociation constants (k_{off}) were calculated from the dissociation half-lives ($t_{1/2}$) of the complexes. With half-lives ranging from 27–820 s (Supplementary Figure S14, SI), similar dissociation constants were obtained for all four constructs (k_{off} = 9.4×10^{-4}–2.7×10^{-2} s^{-1}). Remarkably, the duplexes exhibiting faster Hg^{II} dissociation (such as **X15** ^{DMA}**T**–C) also exhibited more rapid Hg^{II} association. The ratios of dissociation and association rate constants ($k_{off}/k_{on} = K_d$) were therefore nearly identical for all four constructs evaluated (K_d = 10–32 nM, Table 2).

Equilibrium measurements of C–Hg^{II}–T formation

To further evaluate the thermodynamic parameters of C–Hg^{II}–T formation, the changes in fluorescence intensities of 21-mer duplex DNA **X13** or **X15** containing a single ^{DMA}**T**–C mismatch, ^{DMA}**C**–T mismatch, or a wild-type C–T mismatch placed adjacent to a ^{DMA}**C**–G base pair were monitored as a function of Hg^{II} concentration following 1 h equilibration at 4 or 25°C (Figure 6A, Supplementary Figures S15–S18, SI). K_d values were calculated from equilibrium quenching data with the assumption of 1:1 binding stoichiometry by curve-fitting the raw data to mono- or biphasic binding curves (eq 8–12, SI). Duplexes lacking any base pair mismatch and containing a ^{DMA}**C**–G base pair exhibited a mono-phasic 'non-specific' binding curve with a modest apparent affinity of K_d = 2.3 ± 0.1 μM (green tri-

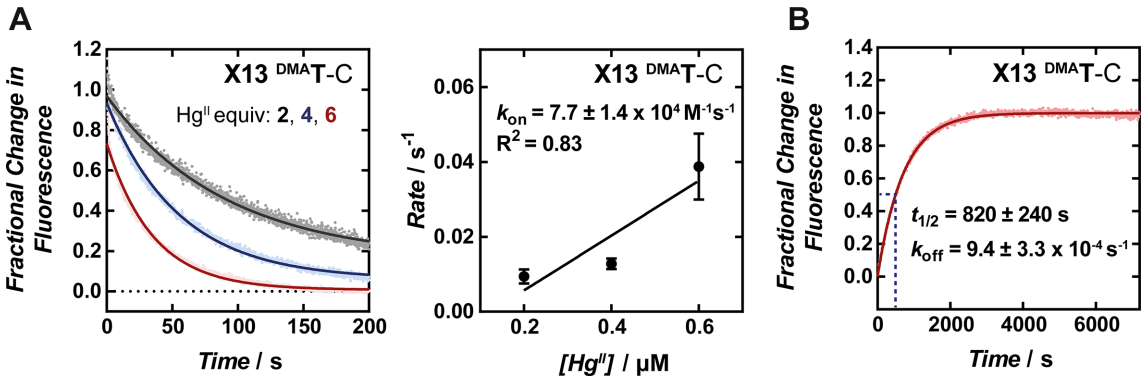

Figure 5. (**A**) Representative fluorescence data showing the time-dependent quenching of **X13** ^{DMA}**T**–C upon addition of 2, 4 or 6 equiv of Hg^{II}. See Supplementary Figure S10, SI for the data and fits obtained for all other duplexes. Association rate constants (k_{on}) were determined by plotting the reaction rates versus Hg^{II} concentration. (**B**) Representative data showing dissociation of Hg^{II} from **X13** ^{DMA}**T**–Hg^{II}–C upon addition 50 equiv of unlabeled, C–T-containing 'scavenger' duplex DNA. See Supplementary Figure S14, SI for data obtained using the other duplexes. C–Hg^{II}–T base pairs were formed by pre-incubation of the DNA with 2 equiv of $Hg(ClO_4)_2$ for 3 h prior to addition of the Hg^{II} 'scavenger' DNA. All samples were excited at 370 nm and fluorescence was monitored at 500–510 nm. Samples contained either 0.1 μM (k_{on}) or 4 μM (k_{off}) of duplex DNA in aqueous buffer (200 mM Na_2HPO_4, 100 mM citric acid and 100 mM $NaNO_3$, pH 7.35).

Table 2. Rate constants of association (k_{on}), dissociation (k_{off}) and calculated equilibrium dissociation constants ($K_d = k_{off}/k_{on}$) of Hg^{II} binding to ^{DMA}**T**–C,^{DMA}**C**–T or C–T in duplex DNA[a]

Sequence	k_{on} (M^{-1} s^{-1})	k_{off} (s^{-1})	K_d (nM)[b]
X13 ^{DMA}**T**–C	$7.7 \pm 1.4 \times 10^4$	$9.4 \pm 3.3 \times 10^{-4}$	12 ± 5.0
X15 ^{DMA}**T**–C	$8.5 \pm 6.7 \times 10^5$	$2.7 \pm 0.5 \times 10^{-2}$	32 ± 26
X15 ^{DMA}**C**–T	$2.3 \pm 1.0 \times 10^5$	$2.2 \pm 0.5 \times 10^{-3}$	10 ± 5.0
X15^{DMA}**C**-G, **X14** C–T	$7.6 \pm 0.8 \times 10^4$	$1.4 \pm 0.2 \times 10^{-3}$	18 ± 3.0

[a] Reported values = mean ± standard deviation from three independent measurements. Dissociation rate constants were determined by addition of 50 equiv of unlabeled DNA. For duplex sequences see Supplementary Table S1, SI.
[b] Equilibrium dissociation constants (K_d) calculated as $K_d = k_{off}/k_{on}$.

Table 3. Steady-state equilibrium dissociation constants (K_d) of Hg^{II} binding to ^{DMA}**T**–C,^{DMA}**C**–T, ^{DMA}T–T or wild-type C–T in duplex DNA[a]

Sequence	Temperature	K_d (nM) non-specific[b]	K_d (nM) mismatch specific[c]
X13 ^{DMA}**T**–C	25°C	-	152 ± 4
X13 ^{DMA}**T**–C	15°C	-	107 ± 4
X13 ^{DMA}**T**–C	4°C	-	56 ± 4
X15 ^{DMA}**T**–C	25°C	1300 ± 300	123 ± 76
X15 ^{DMA}**C**–T	25°C	2300 ± 300	153 ± 27
X15 ^{DMA}**C**–G, **X14** C–T	25°C	2200 ± 400	107 ± 45
X15 ^{DMA}**C**–G	25°C	2260 ± 130	-
X13^{DMA}**T**–T	25°C	-	77 ± 4
X13^{DMA}**T**–T	15°C	-	122 ± 11
X13^{DMA}**T**–T	4°C	-	144 ± 27

[a] Reported values = mean ± standard deviation from three independent measurements. Samples contained 25 nM of DNA in an aqueous buffer containing 200 mM Na_2HPO_4, 100 mM citric acid and 100 mM $NaNO_3$ (pH 7.35). K_d values were calculated by fitting quenching data to either a monoexponential curve (eq 11, SI) or to a biphasic curve (eq 12, SI). All R^2 values were ≥ 0.97 (Supplementary Figures S16 and S17, SI). For duplex sequences see Supplementary Table S1, SI.
[b] Represents local, mismatch-independent binding to duplex DNA.
[c] Represents local, mismatch-dependent binding to duplex DNA.

angles Figure 6B, Table 3). Similar results were previously obtained for duplexes containing ^{DMA}**T**–A and lacking a base pair mismatch (29). Duplexes containing a ^{DMA}**C**–G base pair placed adjacent to a wild-type C–T mismatch exhibited a bi-phasic binding curve (Figure 6B), with a low affinity component having the same apparent affinity as the non-specific binding (K_d (1) = 2.2 ± 0.4 μM) and a high-affinity component (K_d (2) = 107 ± 45 nM, Table 3) exhibiting a similar affinity as determined from the ratio of kinetic rate constants (Table 2). Similar values were obtained for the duplexes containing a single ^{DMA}**T**–C, ^{DMA}**C**–T or ^{DMA}**T**–T mismatch (Table 3, Supplementary Figures S16 and S17, SI). These results demonstrate that Hg^{II} exhibits high affinity for C–T mismatches in duplex DNA–even in the high salt, metal-coordinating buffer conditions (200 mM of Na_2HPO_4, 100 mM of citric acid and 100 mM $NaNO_3$ (pH 7.35)) that were previously shown to minimize non-specific binding interactions with duplex DNA (29).

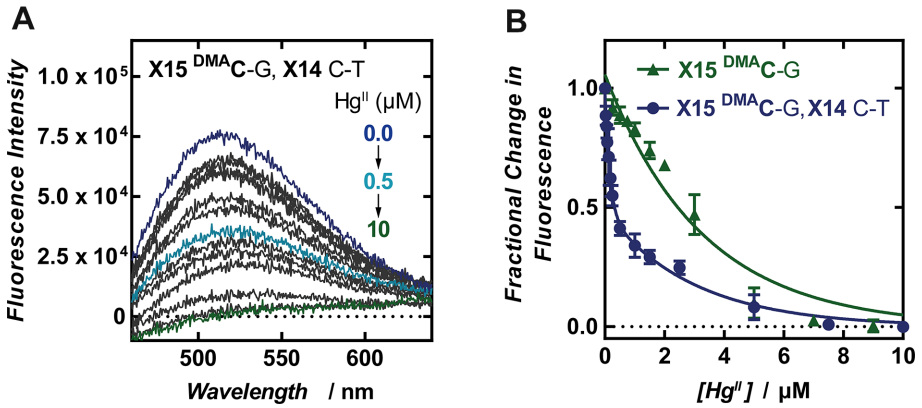

Figure 6. (**A**) Equilibrium fluorescence of **X15** ^{DMA}**C**–G, **X14** C–T upon addition of Hg^{II}. Fluorescence spectra (λ_{ex} = 370 nm) of ^{DMA}**C**-containing sequences in the absence (dark blue) and in the presence of variable concentrations of Hg^{II}. (**B**) Fluorescence quenching of **X15** ^{DMA}**C**–G and **X15** ^{DMA}**C**–G, **X14** C–T fit to a monoexponential (eq 11, SI) or biphasic curve (eq 12, SI), respectively. Samples contained 25 nM duplex DNA in aqueous buffer (200 mM of Na_2HPO_4, 100 mM of citric acid and 100 mM $NaNO_3$ (pH 7.35)) and were equilibrated with variable concentrations of $Hg(ClO_4)_2$ at 25°C for 1 h prior to measuring.

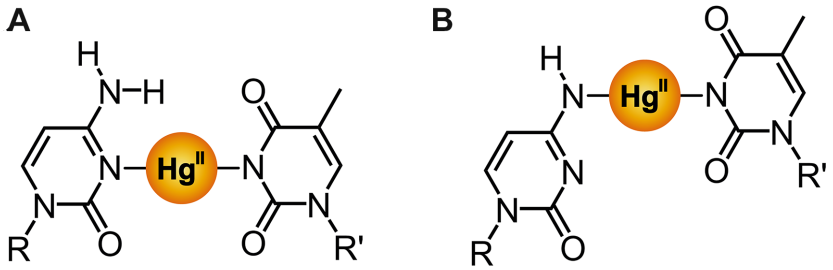

Figure 7. (**A**) Structure of proposed, hypothetical (*N3*)C–Hg^{II}–(*N3*)T coordination complex (36) based upon structural analogy with T–Hg^{II}–T (4,37) and C–Ag^{I}–C (5,8,10). (**B**) Structure of (*N4*)C–Hg^{II}–(*N3*)T coordination complex recently observed in an X-ray crystal structure of a short, A-form duplex DNA containing a C–T mismatch bound to Hg^{II} (9). (R, R' = duplex DNA).

Temperature-dependent K_d measurements revealed that the specific binding affinities of ^{DMA}**T**–C mismatches to Hg^{II} are three-fold higher at 4°C (K_d = 56 nM) than at 25°C (K_d = 152 nM, Table 3). In contrast, ^{DMA}T–T mismatches exhibited a two-fold lower affinity for Hg^{II} at 4°C (K_d = 144 nM) than at 25°C (K_d = 77 nM, Table 3). This latter result is consistent with the positive entropy of formation (ΔS) previously reported for T–Hg^{II}–T base pairs determined using isothermal titration calorimetry (44). By plotting the free energies of formation (ΔG) calculated from K_d measurements at 4°C and 25°C, and assuming a constant enthalpy change (ΔH) over this small temperature range, our data suggest that the formation of C–Hg^{II}–T base pairs involve very little or no positive entropy change, whereas the formation of T–Hg^{II}–T base pairs exhibit a relatively large positive entropy change (Supplementary Figure S18, SI).

DISCUSSION

Here we report the use of fluorescent nucleobase analogs ^{DMA}**T** and ^{DMA}**C** for the characterization of site-selective Hg^{II} binding to C–T mismatches in duplex DNA. Our fluorescence and ^{1}H NMR data revealed that Hg^{II} selectively and stoichiometrically binds to C–T mismatches with high affinity (K_d = 10–153 nM). These affinities are very similar to those for Hg^{II} binding to T–T mismatches under the same conditions (Table 3 and reference (29)). Unlike the widely studied T–Hg^{II}–T metallo base pair, C–Hg^{II}–T formation was previously undetected by thermal melting temperature analyses (44). Despite the high-affinity binding, little or no increase in T_m was observed for duplexes containing C–T mismatches upon addition of Hg^{II} (Table 1 and Supplementary Table S4, SI). This apparent contradiction is likely a result of the lower Hg^{II} affinity to C–T mismatches at higher temperatures (Table 3). These results highlight the fact that ΔT_m values must be interpreted with great caution, and that fluorescent nucleobase analogs offer attractive alternatives for the identification and isothermal study of DNA-metal binding interactions.

Despite their similar equilibrium binding affinities, there are some notable differences between the formation of T–Hg^{II}–T and C–Hg^{II}–T metallo base pairs in duplex DNA. According to temperature-dependent K_d measurements, the ΔS of formation of C–Hg^{II}–T is much smaller than the ΔS of formation of T–Hg^{II}–T (Supplementary Figure S18, SI). The unusual positive ΔS of T–Hg^{II}–T formation was previously ascribed to the release of water molecules from Hg^{II} upon DNA binding (6,44). The smaller ΔS of C–Hg^{II}–T formation therefore suggests less water is released from Hg^{II} upon binding C–T mismatches as compared to T–T mismatches. Consistent with this, C–T mismatches exhibited approximately 10-fold higher rate constants of Hg^{II} association and dissociation as compared to T–T mismatches, sug-

gesting a kinetically less stable, more solvent-exposed coordination site of Hg^{II} in C–Hg^{II}–T than in T–Hg^{II}–T. Taken together, these observations are consistent with a recently reported X-ray structure of a C–Hg^{II}–T base pair in an A-form duplex DNA (9) where the metal ion was unexpectedly bound to the exocyclic amine (*N4*) of a deprotonated cytosine residue and to the *N3* of a deprotonated thymidine (Figure 7). Additional studies using ^{15}N-NMR (4,5) will be required to determine if one or both of these metal binding modes are present in duplex DNA containing C–Hg^{II}–T base pairs in solution.

SUPPLEMENTARY DATA

Supplementary Data are available at NAR Online.

ACKNOWLEDGEMENTS

We are grateful to the University of Zurich and to Prof. Ben Schuler and his group for their technical assistance.

FUNDING

Swiss National Science Foundation [165949]. Funding for open access charge: Swiss National Science.
Conflict of interest statement. None declared.

REFERENCES

1. Yamane,T. and Davidson,N. (1961) On the complexing of desoxyribonucleic acid (DNA) by mercuric ion. *J. Am. Chem. Soc.*, **83**, 2599–2607.
2. Katz,S. (1962) Mechanism of the reaction of polynucleotides and Hg^{II}. *Nature*, **194**, 569.
3. Katz,S. (1963) The reversible reaction of Hg(II) and double-stranded polynucleotides a step-function theory and its significance. *Biochim. Biophys. Acta*, **68**, 240–253.
4. Tanaka,Y., Oda,S., Yamaguchi,H., Kondo,Y., Kojima,C. and Ono,A. (2007) ^{15}N-^{15}N *J*-coupling across Hg^{II}: Direct observation of Hg^{II}-mediated T–T base pairs in a DNA duplex. *J. Am. Chem. Soc.*, **129**, 244–245.
5. Dairaku,T., Furuita,K., Sato,H., Šebera,J., Nakashima,K., Kondo,J., Yamanaka,D., Kondo,Y., Okamoto,I., Ono,A. *et al.* (2016) Structure determination of an Ag^{I}-mediated cytosine-cytosine base pair within DNA duplex in solution with ^{1}H/^{15}N/^{109}Ag NMR spectroscopy. *Chem. Eur. J.*, **22**, 13028–13031.
6. Yamaguchi,H., Sebera,J., Kondo,J., Oda,S., Komuro,T., Kawamura,T., Dairaku,T., Kondo,Y., Okamoto,T., Ono,A. *et al.* (2014) The structure of metallo-DNA with consecutive thymine-Hg^{II}-thymine base pairs explains positive entropy for the metallo base pair. *Nucleic Acids Res.*, **42**, 4094–4099.
7. Kondo,J., Yamada,T., Hirose,C., Okamoto,I., Tanaka,Y. and Ono,A. (2014) Crystal structure of metallo DNA duplex containing consecutive Watson-Crick-like T–Hg(II)-T base pairs. *Angew. Chem. Int. Ed.*, **53**, 2385.
8. Kondo,J., Tada,Y., Dairaku,T., Hattori,Y., Saneyoshi,H., Ono,A. and Tanaka,Y. (2017) A metallo-DNA nanowire with interrupted one-dimensional silver array. *Nat. Chem.*, **9**, 956–960.
9. Liu,H., Cai,C., Haruehanroengra,P., Yao,Q., Chen,Y., Yang,C., Luo,Q., Wu,B., Li,J., Ma,J. *et al.* (2017) Flexibility and stabilization of Hg^{II}-mediated C:T and T:T base pairs in DNA duplex. *Nucleic Acids Res.*, **45**, 2910–2918.
10. Hehua,L., Shen,F., Haruehanroengra,P., Yao,Q., Cheng,Y., Chen,Y., Yang,C., Zhang,J., Wu,B., Luo,Q. *et al.* (2017) A DNA structure containing Ag^{I}-mediated G:G and C:C base pairs. *Angew. Chem. Int. Ed.*, **56**, 9430–9434.
11. Ennifar,E., Walter,P. and Dumas,P. (2003) A crystallographic study of the binding of 13 metal ions to two related RNA duplexes. *Nucleic Acids Res.*, **31**, 2671–2682.
12. Liu,J. and Lu,Y. (2007) Rational design of "turn-on" allosteric DNAzyme catalytic beacons for aqueous mercury ions with ultrahigh sensitivity and selectivity. *Angew. Chem. Int. Ed.*, **46**, 7587–7590.
13. Lin,Y.-W., Ho,H.-T., Huang,C.-C. and Chang,H.-T. (2008) Fluorescence detection of single nucleotide polymorphisms using a universal molecular beacon. *Nucleic Acids Res.*, **36**, e123.
14. Mor-Piperberg,G., Tel-Vered,R., Elbaz,J. and Willner,I. (2010) Nanoengineered electrically contacted enzymes on DNA scaffolds: Functional assemblies for the selective analysis of Hg^{2+} ions. *J. Am. Chem. Soc.*, **132**, 6878–6879.
15. Park,K.S., Jung,C. and Park,H.G. (2010) "Illusionary" polymerase activity triggered by metal ions: use for molecular logic-gate operations. *Angew. Chem. Int. Ed.*, **49**, 9757–9760.
16. Wang,Z.-G., Elbaz,J. and Willner,I. (2011) DNA machines: bipedal walker and stepper. *Nano Lett.*, **11**, 304–309.
17. Wen,S., Zeng,T., Liu,L., Zhao,K., Zhao,Y., Liu,X. and Wu,H.-C. (2011) Highly sensitive and selective DNA-based detection of mercury(II) with α-hemolysin nanopore. *J. Am. Chem. Soc.*, **133**, 18312–18317.
18. Thomas,J.M., Yu,H.-Z. and Sen,D. (2012) A mechano-electronic DNA switch. *J. Am. Chem. Soc.*, **134**, 13738–13748.
19. Xiao,S.J., Hu,P.P., Xiao,G.F., Wang,Y., Liu,Y. and Huang,C.Z. (2012) Label-free detection of prion protein with its DNA aptamer through the formation of T–Hg^{2+}–T configuration. *J. Phys. Chem. B*, **116**, 9565–9569.
20. Kang,I., Wang,Y., Reagan,C., Fu,Y., Wang,M.X. and Gu,L.-Q. (2013) Designing DNA interstrand lock for locus-specific methylation detection in a nanopore. *Sci. Rep.*, **3**, 2381.
21. Bi,S., Ji,B., Zhang,Z. and Zhu,J.-J. (2013) Metal ions triggered ligase activity for rolling circle amplification and its application in molecular logic gate operations. *Chem. Sci.*, **4**, 1858–1863.
22. Wang,Y., Ritzo,B. and Gu,L.-Q. (2015) Silver(I) ions modulate the stability of DNA duplexes containing cytosine, methylcytosine and hydroxymethylcytosine at different salt concentrations. *RSC Adv.*, **5**, 2655–2658.
23. Park,K.S., Lee,C.Y. and Park,H.G. (2016) Metal ion triggers for reversible switching of DNA polymerase. *Chem. Commun.*, **52**, 4868–4871.
24. Hong,T., Yuan,Y., Wang,T., Ma,J., Yao,Q., Hua,X., Xia,Y. and Zhou,X. (2017) Selective detection of N6-methyladenine in DNA *via* metal ion-mediated replication and rolling circle amplification. *Chem. Sci.*, **8**, 200–205.
25. Guo,X. and Seela,F. (2017) Anomeric 2′-deoxycytidines and silver ions: hybrid base pairs with greatly enhanced stability and efficient DNA mismatch detection with α-dC. *Chem. Eur. J.*, **23**, 11776–11779.
26. Urata,H., Yamaguchi,E., Funai,T., Matsumura,Y. and Wada,S.-I. (2010) Incorporation of thymine nucleotides by DNA polymerases through T–Hg^{II}–T base pairing. *Angew. Chem. Int. Ed.*, **49**, 6516–6519.
27. Funai,T., Miyazaki,Y., Aotani,M., Yamaguchi,E., Nakagawa,O., Wada,S.-I., Torigoe,H., Ono,A. and Urata,H. (2012) Ag^{I} ion mediated formation of a C-A mispair by DNA polymerases. *Angew. Chem. Int. Ed.*, **51**, 6464–6466.
28. Funai,T., Nakamura,J., Miyazaki,Y., Kiriu,R., Nakagawa,O., Wada,S.-I., Ono,A. and Urata,H. (2014) Regulated incorporation of two different metal ions into programmed sites in a duplex by DNA polymerase catalyzed primer extension. *Angew. Chem. Int. Ed.*, **53**, 6624–6627.
29. Schmidt,O.P., Mata,G. and Luedtke,N.W. (2016) Fluorescent base analogue reveals T–Hg^{II}–T base pairs have high kinetic stabilities that perturb DNA metabolism. *J. Am. Chem. Soc.*, **138**, 14733–14739.
30. Clever,G.H., Kaul,C. and Carell,T. (2007) DNA-metal base pairs. *Angew. Chem. Int. Ed.*, **46**, 6226–6236.
31. Takezawa,Y. and Shionoya,M. (2012) Metal-mediated DNA base pairing: alternatives to hydrogen-bonded Watson–Crick base pairs. *Acc. Chem. Res.*, **45**, 2066–2076.
32. Scharf,P. and Müller,J. (2013) Nucleic acids with metal-mediated base pairs and their application. *ChemPlusChem*, **78**, 20–34.
33. Tanaka,Y., Kondo,J., Sychrovský,V., Šebera,J., Dairaku,T., Saneyoshi,H., Urata,H., Torigoe,H. and Ono,A. (2015) Structures, physiochemical properties, and applications of T–Hg^{II}–T, C-Ag^{I}-C, and other metallo-base-pairs. *Chem. Commun.*, **51**, 17343–17360.
34. Takezawa,Y., Müller,J. and Shionoya,M. (2017) Artificial DNA base pairing mediated by diverse metal ions. *Chem. Lett.*, **46**, 622–633.

35. Jash,B. and Müller,J. (2017) Metal-mediated base pairs: from characterization to application. *Chem. Eur. J.*, **23**, 17166–17178.
36. Ono,A., Torigoe,H., Tanaka,Y. and Okamoto,I. (2011) Binding of metal ions by pyrimidine base pairs in DNA duplexes. *Chem. Soc. Rev.*, **40**, 5855–5866.
37. Tanaka,Y., Yamaguchi,H., Oda,S., Kondo,Y., Nomura,M., Kojima,C. and Ono,A. (2006) The structure of metallo-DNA with consecutive thymine-Hg^{II}-thymine base pairs explains positive entropy for the metallo base pair formation. *Nucleic Acids Res.*, **42**, 613–624.
38. Miyake,Y., Togashi,H., Tashiro,M., Yamaguchi,H., Oda,S., Kudo,M., Tanaka,Y., Kondo,Y., Sawa,R., Fujimoto,T. *et al.* (2006) $Mercury^{II}$-mediated formation of thymine-Hg^{II}-thymine base pairs in DNA duplexes. *J. Am. Chem. Soc.*, **128**, 2172–2173.
39. Ono,A., Cao,S., Togashi,H., Tashiro,M., Fujimoto,T., Machinami,T., Oda,S., Miyake,Y., Okamoto,I. and Tanaka,Y. (2008) Specific interactions between silver(I) ions and cytosine-cytosine pairs in DNA duplexes. *Chem. Commun.*, 4825–4827.
40. Torigoe,H., Miyakawa,Y., Ono,A. and Kozasa,T. (2011) Thermodynamic properties of the specific binding between Ag^+ ions and C:C mismatched base pairs in duplex DNA. *Nucleosides Nucleotides Nucleic Acids*, **30**, 149–167.
41. Torigoe,H., Miyake,Y., Ono,A. and Kozasa,T. (2012) Positive cooperativity of the specific binding between Hg^{2+} ion and T:T mismatched base pairs in duplex DNA. *Thermochim. Acta*, **532**, 28–35.
42. Torigoe,H., Okamoto,I., Dairaku,T., Tanaka,Y., Ono,A. and Kozasa,T. (2012) Thermodynamic and structural properties of the specific binding between Ag^+ ion and C:C mismatched base pair in duplex DNA to form C-Ag-C metal-mediated base pair. *Biochimie*, **94**, 2431–2440.
43. Mata,G., Schmidt,O.P. and Luedtke,N.W. (2016) A fluorescent surrogate of thymidine in duplex DNA. *Chem. Commun.*, **52**, 4718–4721.
44. Torigoe,H., Ono,A. and Kozasa,T. (2010) Hg^{II} ion specifically binds with T:T mismatched base pairs in duplex DNA. *Chem. Eur. J.*, **16**, 13218–13225.
45. Hofr,C. and Brabec,V. (2001) Thermal and thermodynamic properties of duplex DNA containing site-specific interstrand cross-link of antitumor cisplatin or its clinically ineffective trans isomer. *J. Biol. Chem.*, **276**, 9655–9661.
46. Rodriguez-Ramos,M.M. and Wilker,J.J. (2010) Metal-bipyridine complexes in DNA backbones and effects on thermal stability. *J. Biol. Inorg. Chem.*, **15**, 629–639.
47. Fedoriw,A.M., Liu,H., Anderson,V.E. and deHaseth,P.L. (1998) Equilibrium and kinetic parameters of the sequence-specific interaction of *Escherichia coli* RNA polymerase with nontemplate strand oligodeoxyribonucleotides. *Biochemistry*, **37**, 11971–11979.
48. Arzumanov,A., Godde,F., Moreau,S., Toulmé,J.-J., Weeds,A. and Gait,M.J. (2000) Use of the fluorescent nucleoside analogue benzo[g]quinazoline 2′-*O*-methyl-*β*-D-ribofuranoside to monitor the binding of the HIV-1 Tat protein or of antisense oligonucleotides to the TAR RNA stem-loop. *Helv. Chim. Acta*, **83**, 1424–1436.
49. Bradrick,T.D. and Marino,J.P. (2004) Ligand-induced changes in 2-aminopurine fluorescence as a probe for small molecule binding to HIV-1 TAR RNA. *RNA*, **10**, 1459–1468.
50. Gilbert,S.D., Stoddard,C.D., Wise,S.J. and Batey,R.T. (2006) Thermodynamic and kinetic characterization of ligand binding to the purine riboswitch aptamer domain. *J. Mol. Biol.*, **359**, 754–768.
51. Kimura,T., Kawai,K., Fujitsuka,M. and Majima,T. (2007) Monitoring G-quadruplex structures and G-quadruplex-ligand complex using 2-aminopurine modified oligonucleotides. *Tetrahedron*, **63**, 3585–3590.
52. Parsons,J. and Hermann,T. (2007) Conformational flexibility of ribosomal decoding-site RNA monitored by fluorescent pteridine base analogues. *Tetrahedron*, **63**, 3548–3552.
53. Lang,K., Rieder,R. and Micura,R. (2007) Ligand-induced folding of the *thiM* TPP riboswitch investigated by a structure-based fluorescence spectroscopic approach. *Nucleic Acids Res.*, **35**, 5370–5378.
54. Barbieri,C.M., Kaul,M. and Pilch,D.S. (2007) Use of 2-aminopurine as a fluorescent tool for characterizing antibiotic recognition of the bacterial rRNA A-site. *Tetrahedron*, **63**, 3567–6574.
55. Xie,Y., Dix,A.V. and Tor,Y. (2009) FRET enabled real time detection of RNA-small molecule binding. *J. Am. Chem. Soc.*, **131**, 17605–17614.
56. Velmurugu,Y., Chen,X., Sevilla,P.S., Min,J.-H. and Ansari,A. (2016) Twist-open mechanism of DNA damage recognition by the Rad4/XPC nucleotide excision repair complex. *Proc. Natl. Acad. Sci. U.S.A.*, **113**, E2296–E2305.
57. Kim,S.J. and Kool,E.T. (2006) Sensing metal ions with DNA building blocks: fluorescent pyridobenzimidazole nucleosides. *J. Am. Chem. Soc.*, **128**, 6164–6171.
58. Dumas,A. and Luedtke,N.W. (2012) Site-specific control of *N*7-metal coordination in DNA by a fluorescent purine derivative. *Chem. Eur. J.*, **18**, 245–254.
59. Omumi,A., McLaughlin,C.K., Ben-Israel,D. and Manderville,R.A. (2012) Application of a fluorescent *C*-linked phenolic purine adduct for selective N7-metalation of DNA. *J. Phys. Chem. B*, **116**, 6158–6165.
60. Jana,S.K., Guo,X., Mei,H. and Seela,F. (2015) Robust silver-mediated imidazolo-dC base pairs in metal DNA: dinuclear silver bridges with exceptional stability in double helices with parallel and antiparallel strand orientation. *Chem. Commun.*, **51**, 17301–17304.
61. Mata,G. and Luedtke,N.W. (2015) A fluorescent probe for proton-coupled folding reveals slow exchange of i-motif and duplex DNA. *J. Am. Chem. Soc.*, **137**, 699–707.
62. Schulhof,J.C., Molko,D. and Teoule,R. (1987) The final deprotection step in oligonucleotide synthesis is reduced to a mild and rapid ammonia treatment by using labile base-protecting groups. *Nucleic Acids Res.*, **15**, 397–416.
63. Cantor,C.R., Warshaw,M.M. and Shapiro,H. (1970) Oligonucleotide interactions. III. Circular dichroism studies of the conformation of deoxyoligonucleotides. *Biopolymers*, **9**, 1059–1077.
64. Borer,P.N. (1975) Optical properties of nucleic acids, absorption and circular dichroism spectra. In: Fasman,GD (ed). *Handbook of Biochemistry and Molecular Biology: Nucleic Acids*. 3rd edn., CRC Press, Cleveland, Ohio, Vol. **1**, pp. 589–595.
65. Brown,T. and Brown,D.J.S. (1991) Modern machine-aided methods of oligodeoxyribonucleotide synthesis. In: Eckstein,F (ed). *Oligonucleotides and Analogues. A practical approach*. IRL Press, Oxford, pp. 1–24.
66. Bhaumik,S.R., Chary,K.V.R., Govil,G., Liu,K. and Miles,H.T. (1997) Homopurine and homopyrimidine strands complementary in parallel orientation form an antiparallel duplex at neutral pH with A-C,G-T, and T-C mismatched base pairs. *Biopolymers*, **41**, 773–784.
67. Allawi,H.T. and SantaLucia,J. Jr (1998) Thermodynamics of internal C•T mismatches in DNA. *Nucleic Acids Res.*, **26**, 2694–2701.